

A HIGH RESOLUTION STUDY OF THE DISTRIBUTION AND MOTIONS OF NEUTRAL HYDROGEN IN THE SMALL CLOUD OF MAGELLAN

By J. V. HINDMAN*

[Manuscript received November 18, 1966]

Summary

Observations of radiation from neutral hydrogen in the Small Cloud of Magellan at a wavelength of 21 cm have been made using the 210 ft Parkes telescope and a multichannel receiver. Profiles were observed over an area of 30 sq deg of sky.

There is good correlation between the distribution of the neutral gas and the bright stars, but no detailed correspondence with clusters or Cepheids has been found.

Well-defined structure is evident in the velocity distribution of the gas, which is interpreted as originating in a number of expanding gas shells between 1 and 2 kpc in diameter and containing from 1 to $2 \times 10^7 M_{\odot}$ of neutral hydrogen.

A rotation curve has been derived and the total mass of the SMC estimated at $1.5 \times 10^9 M_{\odot}$, while the corresponding mass of neutral hydrogen in the system is $5 \times 10^8 M_{\odot}$.

I. INTRODUCTION

The first reported detection of 21 cm line radiation from the Magellanic Clouds by Kerr, Hindman, and Robinson (1954) showed a surprisingly large amount of neutral hydrogen associated with these nearby irregular galaxies, particularly for the Small Cloud, which, on reasonable estimates of the overall mass, appeared to contain 20% neutral hydrogen. Using a more sensitive receiver Hindman, Kerr, and McGee (1963) and Hindman *et al.* (1963) confirmed the high gas content.

Because of the poor aerial resolution in these earlier observations ($1^{\circ} \cdot 5$ and $2^{\circ} \cdot 2$), equivalent to regions $1\frac{1}{2}$ – $2\frac{1}{2}$ kpc in diameter at the distance of the Small Magellanic Cloud (SMC), very little detail in the gas distribution was revealed, though in the second survey it was apparent, owing to the increased receiver sensitivity and frequency stability, that many of the line profiles were multi-peaked. This possibility had earlier been suggested by Johnson (1961) from the original data of Kerr, Hindman, and Robinson. The quality of the original records, however, was such that confirmation had to await improvements in equipment sensitivity and stability.

The observations reported in the present paper have been made with the Australian National Radio Astronomy Observatory 210 ft telescope at Parkes, N.S.W., and the multichannel receiver described by McGee and Murray (1963). An area of approximately 30 sq deg of sky covering the region of the SMC has been surveyed. Some 4500 profiles were recorded with an aerial resolution of less than $15'$ arc.

* Division of Radiophysics, CSIRO, University Grounds, Chippendale, N.S.W.; present address: Siding Spring Observatory, Coonabarabran, N.S.W.

The results of the survey show that about one-third of the profiles have distinct multiple peaks related to separate condensations of gas in the line of sight moving with different radial velocities, and an examination of the distribution of the velocity features leads to an explanation of their origin in several large expanding shells of gas embedded in the main gas mass associated with the SMC.

The gas distribution is compared with optical and radio continuum distributions, and the previous values for the mass of neutral hydrogen are confirmed.

From the overall velocity distribution a rotation curve has been derived which is then used to estimate the total mass of the SMC, $1.5 \times 10^9 M_{\odot}$. The proportion of neutral hydrogen in the system may be as high as 30% of the total mass.

II. EQUIPMENT AND OBSERVATIONS

(a) *Telescope*

The 210 ft telescope of the Australian National Radio Astronomy Observatory was used for all the observations reported here. For H-line observations the dish is fed by a circular wave guide giving a nearly circular beam $14' \cdot 6$ arc to the half-power points. Sidelobes were not detectable on strong continuum sources, since the dish is underfed and the beam shape is very nearly Gaussian, smearing out the near sidelobes.

Measurements of the ratio of total power in the main lobe and the nearby extensions out to a few degrees from the centre of the main beam, to the total aerial power at the feed, give a value of 0.8. The inverse of this factor is used to convert aerial temperatures to "main beam" or brightness temperature.

For the period of the observations the pointing accuracy of the telescope was better than $1'$ arc in both right ascension and declination.

(b) *Receiver*

The receiver used was fundamentally the same as that used for the earlier $2^{\circ} \cdot 2$ beam survey of the Clouds (Hindman *et al.* 1963). It has been described in detail by McGee and Murray (1963). It has 48 channels $7 \cdot 8$ km/sec wide, spaced at $7 \cdot 0$ km/sec intervals. In addition, a group of 15 channels, $2 \cdot 1$ km/sec wide and spaced at $2 \cdot 0$ km/sec intervals, was available. All observations were recorded using an output time constant of 60 sec in the final detector circuit. With this time constant the r.m.s. noise fluctuations on each channel are less than $\pm 1 \cdot 1$ degK.

The output from the receiver was recorded digitally on punched paper tape, along with aerial position information, and was later processed by the SILLIAC digital computer of the Physics Department at the University of Sydney.

(c) *Calibrations*

The relative temperature sensitivity for each channel and the day-to-day sensitivity of the receiver were checked by means of an argon discharge lamp. Used as a source of wide-band noise and switched to simulate a line signal of equal intensity in all channels of the receiver, the output from the lamp was injected into the feed horn of the receiver.

Periodic checks of high-level profiles during the observing period show that the argon tube is constant in output to better than $\pm 2\%$.

The absolute temperature scale is in terms of an assumed temperature of 10 100°K for the argon discharge source. This may be in error by as much as 10% for an extreme case. For three lamps tested the scatter in the calibration was less than 5%. Brightness temperatures are subject to further uncertainty in the measurement of aerial efficiency, though one may expect that, because of the rather high value obtained, the brightness temperatures quoted will almost certainly be lower limits.

Generally, the results in this paper are in terms of an intensity unit that is equivalent to an aerial temperature of 1.4 degK or a brightness temperature of 1.75 degK.

Frequency calibrations were made using a counter-type frequency meter measuring frequencies at about 38 MHz, and all frequencies were measured to an accuracy that allowed velocities to be calculated to better than ± 0.1 km/sec.

(d) *Observational Method*

(i) *Zero Level*

The multichannel system of detecting and recording line profiles requires that the zero level for each channel should be established under the same conditions as the recorded profile. This often presents considerable difficulty, as there appears to be some gas in whatever direction one chooses to observe. In the case of observations of the Magellanic Clouds, however, the range of frequency covered by the Cloud profiles and the fairly high galactic latitude of the Clouds combine to make it possible to observe a zero baseline in a region not far removed from the SMC. For these observations a point at Dec. -70° and R.A. 00^h 00^m was chosen as the zero reference. The reliability of this point as a zero was checked by exploring the region near this position for variations which would indicate a changing profile. In practice, no variation greater than 0.5 degK was seen in an area of 1 degree square around the check point or in a special series of profiles taken along the R.A. 00^h 00^m line from Dec. -70° to -76° .

(ii) *Constant Declination Tracks*

Most of the observations were taken as constant declination scans, spaced at intervals of 6'. Each scan commenced at R.A. 00^h 00^m and continued to at least 01^h 30^m.

The tracking rate along each constant declination scan was chosen so that the aerial covered 1° of sky in 20 min, i.e. 6' arc every 2 min. A profile was recorded every 2 min, and thus the area from Dec. -70° to -76° and from R.A. 00^h 00^m to 01^h 30^m was covered, recording profiles on a 6' arc grid. Since the aerial beamwidth is 14'.6 arc, the effect of smoothing due to aerial movement was expected to be very small, but comparisons between profiles taken from the tracks and profiles specially recorded with the aerial following a point in the sky do show occasional differences as large as 10% in peak temperature. A total of over 4500 profiles was recorded,

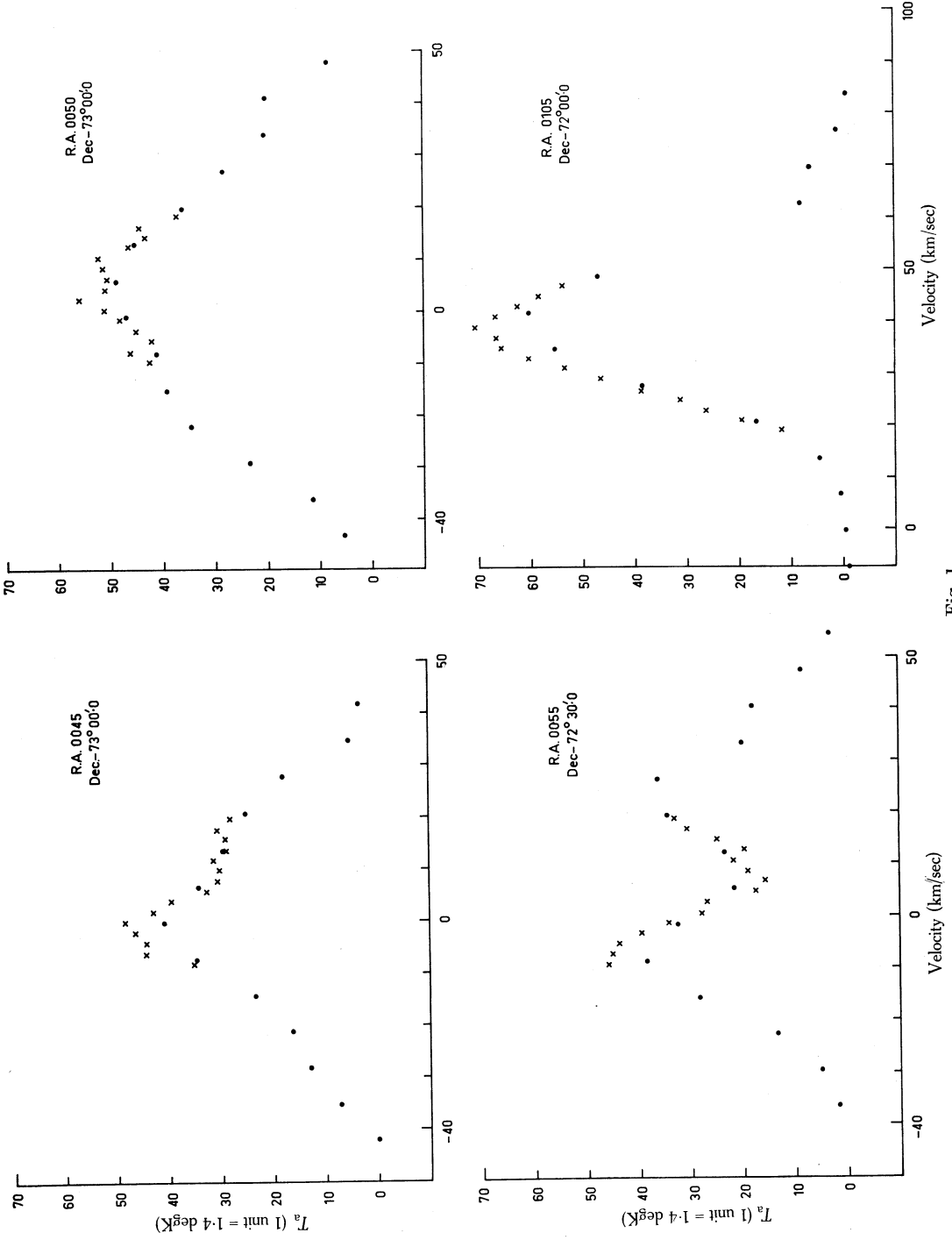


Fig. 1

mainly in two observing periods, one in August 1962 and the other in September 1963. Supplementary observations were made in 1964–65. The observations occupied about 220 hours of telescope time, including calibration of the aerial efficiency.

III. OBSERVATIONAL DATA

The full observational data have been published by Hindman and Balnaves (1967), and selected diagrams are reproduced in the present paper for illustration of the discussion. The essential features of the data are briefly described here.

(a) *Velocity–R.A. Contours (Epoch 1963·0)*

To help in assimilating the very large amount of data involved the profiles have been reduced to a set of contour diagrams, one for each constant declination track. In these diagrams, samples of which are reproduced in Figures 8, 12, 14, and 15, contours of equal intensity are plotted for a constant declination with right ascension and velocity as the coordinates. A vertical section across the contours reproduces the profile for the point in the sky defined by the declination of the track and the right ascension at which the section is taken. The epoch of these diagrams is the mean epoch of observation 1963·0. The contour interval on these diagrams is 5 units, i.e. 7 degK in aerial temperature or 8·8 degK in brightness temperature. The outer contour in each case is an estimate of the limits of detectable radiation and in the present series of observations is at about $T_a = 3^\circ\text{K}$. From these diagrams the structural features of the velocity distributions are most easily discerned.

(b) *Constant Velocity Maps (Epoch 1975)*

The same data have also been presented in the form of contours of equal intensity at constant velocity over the area of the SMC with the same contour interval as for the R.A.–velocity diagrams. The full set of diagrams shows the changing pattern of the hydrogen distribution with change of velocity, and details in the hydrogen distribution at various velocities are highlighted. Figure 3 is an example of this type of diagram at +20 km/sec near the centre of the velocity range covered by the cloud gas.

(c) *Special Sections*

For the purposes of discussion in this paper a number of velocity contour diagrams have been constructed from the original data, which have as sky coordinate some line on the sky other than the constant declination track of the original observations. These are reproduced in Figures 9, 10, 13, and 17 and will be discussed in Sections V and VI(d).

(d) *Velocity Corrections*

All the results used in this paper have been corrected for motion of the observer due to the Earth's orbital motion, the solar motion relative to the local standard of

Fig. 1 (*opposite*).—Comparison of profiles taken with 36 kHz (dots) and 10 kHz (crosses) filter bandwidth.

rest, and motion of the Sun due to rotation about the galactic centre. The velocities are therefore referred to a frame of reference at the position of the Sun and stationary with respect to the galactic centre.

(e) *Narrow-band Data*

Partial profiles were observed in addition to the main set of profiles. These partial profiles were observed at 50 separate points throughout the SMC with a velocity resolution of 2 km/sec, in order to test the likelihood of further detail in the profiles being detected. Figure 1 is a sample showing the comparison between the

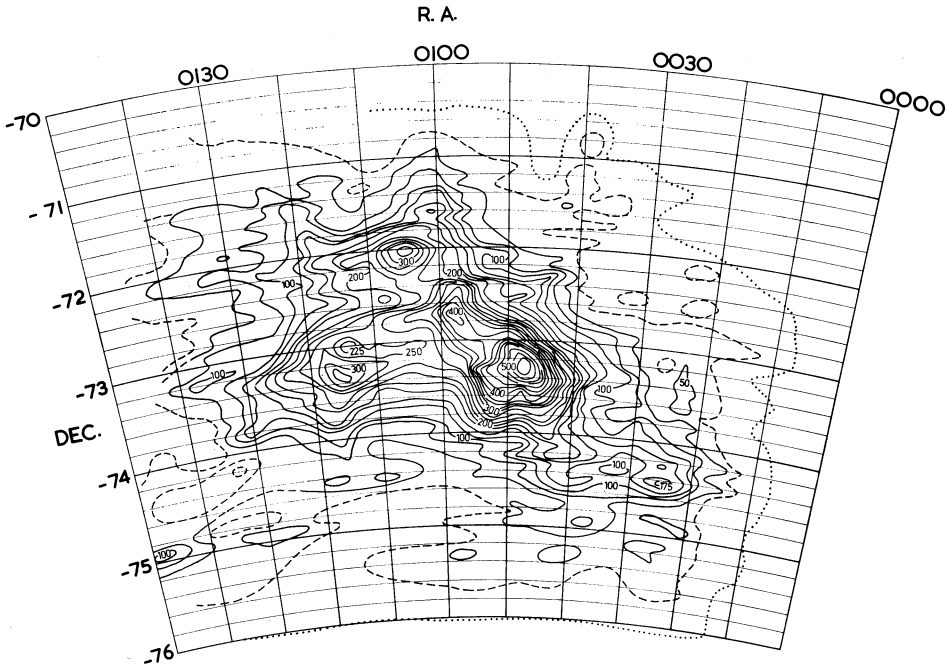


Fig. 2.—Contours of 21 cm H-line integrated brightness over the area of the SMC (contour unit = $3.5 \times 10^{-17} \text{ W m}^{-2} \text{ sr}^{-1}$). The outer (dotted) contour is an estimate of the limits of detectable radiation with the present receiver sensitivity. Epoch of coordinates 1975.

full profiles at 7 km/sec resolution and the partial profile at 2 km/sec resolution. None of the high resolution observations showed any extra detail in the profiles, though in some cases there was a sharpening of the profile peak as in Figure 1. These measurements cannot be taken as indicating that no fine structure exists, but they do indicate that no general modification of the profiles is likely to be observed with greater velocity resolution and the existing aerial resolution.

IV. INTEGRATED BRIGHTNESS CONTOURS (EPOCH 1975)

Figure 2 shows the isophotes of the integrated brightness of 21 cm line radiation over the area of the SMC for epoch 1975.

The integrated brightness is a measure of the total energy received from a given direction and is measured in terms of the area under the line profile. It may be defined as

$$B_{\text{int}} = \frac{2k}{\lambda^2} \int T_\nu d\nu,$$

where k is Boltzmann's constant.

The contour unit is equivalent to a brightness temperature of 1.75 degK over a velocity range of 7 km/sec, equivalent to 3.5×10^{-17} W m⁻² sr⁻¹, and the contours are plotted at intervals of 25 units or 8.7×10^{-16} W m⁻² sr⁻¹.

The above values apply to an ideal filter with a square bandpass examining a profile with a uniform brightness distribution. No correction for the departure of the observations from the ideal conditions was attempted.

A similar map using only the incomplete data from the 1962 series of observations was published by Hindman (1964*a*). One feature of this earlier map at R.A. 01^h 04^m and Dec. $-73^\circ 36' \cdot 0$ proved to be the result of instrumental variations, and this has been eliminated completely. Other changes, relatively minor, are due mainly to the closer grid in the present observations.

(a) *Hydrogen Mass*

With the use of the integrated brightness contours a calculation of the number of atoms in a line-of-sight column of cross-sectional area 1 cm² is possible, as summarized by Kerr, Hindman, and Robinson (1954), thus,

$$N = \frac{1}{2.6 \times 10^{-15}} \int_0^\infty T_\nu d\nu,$$

$$T_\nu = \theta (1 - e^{-\tau}),$$

θ being the excitation temperature of the gas and τ the optical depth.

In previous discussions on the SMC, Kerr, Hindman, and Robinson suggested that the low observed-brightness temperatures and apparent lack of saturation effects in the measured profiles indicated that τ was very small and, thus, that T_ν was unaffected by self-absorption and was a valid representation of the total number of atoms in the line of sight. With improved aerial resolution in the present series of observations, however, much higher temperatures are found in some regions. Moreover, though saturation of the profiles is not apparent it cannot be dismissed, since some structural features have angular sizes of the order of the aerial beam.

For the present observations the maximum measured peak temperature is near 150°K, while except for two small regions peak temperatures are below 50°K for the rest of the Cloud. If we assume that the measured peak temperature is characteristic of the kinetic temperature over the Cloud, then the optical depth will be quite small in general.

The assumption of low optical depth means that the calculated number of atoms in the line of sight is a lower limit. Thus, the total hydrogen masses are also lower limits.

Assuming τ small, then, we have

$$N = 6.2 \times 10^{35} B_{\text{int}},$$

the number of atoms in a column of cross section 1 cm^2 ; and the number of atoms corresponding to an integrated brightness B_{int} over an area of $\delta A \text{ deg}^2$ is

$$\delta N = 6.2 \times 10^{78} B_{\text{int}} \delta A$$

if the distance of the SMC is taken to be 60 kpc (Gascoigne and Kron 1965).

The calculated number of neutral hydrogen atoms for the SMC gas west of R.A. $01^{\text{h}} 40^{\text{m}}$ is 5.6×10^{65} , equivalent to a mass of $4.8 \times 10^8 M_{\odot}$.

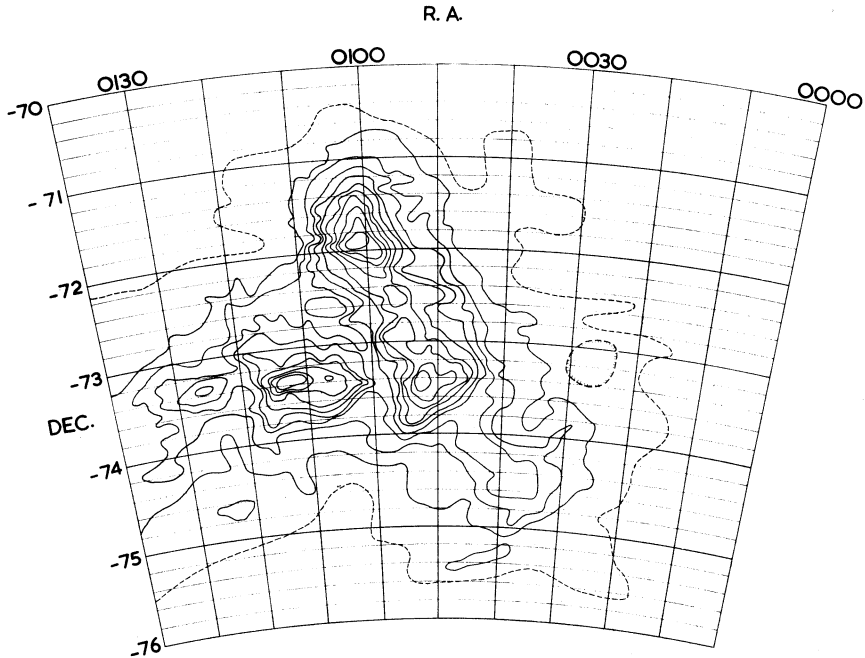


Fig. 3.—Contours of equal intensity of 21 cm line radiation at a velocity $+20 \text{ km/sec}$. The full contours have the values 5, 10, 15, etc. units where 1 unit equals 1.4 degK aerial temperature; the outer (dashed) contour is an estimate of the limits of detectable radiation with the present receiver sensitivity. Epoch of coordinates 1975.

After applying corrections for the different assumed distances this figure may be compared with $6.5 \times 10^8 M_{\odot}$ for the whole of the SMC gas, including a substantial amount of gas from the link region between the Cloud extending to R.A. $03^{\text{h}} 00^{\text{m}}$, found by Kerr, Hindman, and Robinson (1954). Hindman, Kerr, and McGee (1963) have given a figure of $4.6 \times 10^8 M_{\odot}$ for the gas judged to be in the main body of the Cloud and excluding the link.

Comparison of the mass of neutral hydrogen in the SMC, $4.8 \times 10^8 M_{\odot}$, with the most recent figure for the Large Magellanic Cloud (LMC), $5.4 \times 10^8 M_{\odot}$ (McGee and Milton 1966), once again accentuates the very high gas content of the SMC.

(b) *Distribution of HI and the Correlation with Optical Components*(i) *HI Distribution and HII Regions*

The gas in the SMC is fairly smoothly distributed. Only three major concentrations appear in the integrated gas distribution in Figure 2. All three are represented on most of the constant velocity maps, of which Figure 3 is an example. The peak temperatures in the concentrations are 100, 110, and 150°K, while the peaks in the surrounding regions are of the order of 30–50°K. Thus, the concentrations are merged into a fairly high level background. The best estimates of diameters for the concentrations is of the order of 500–600 pc.

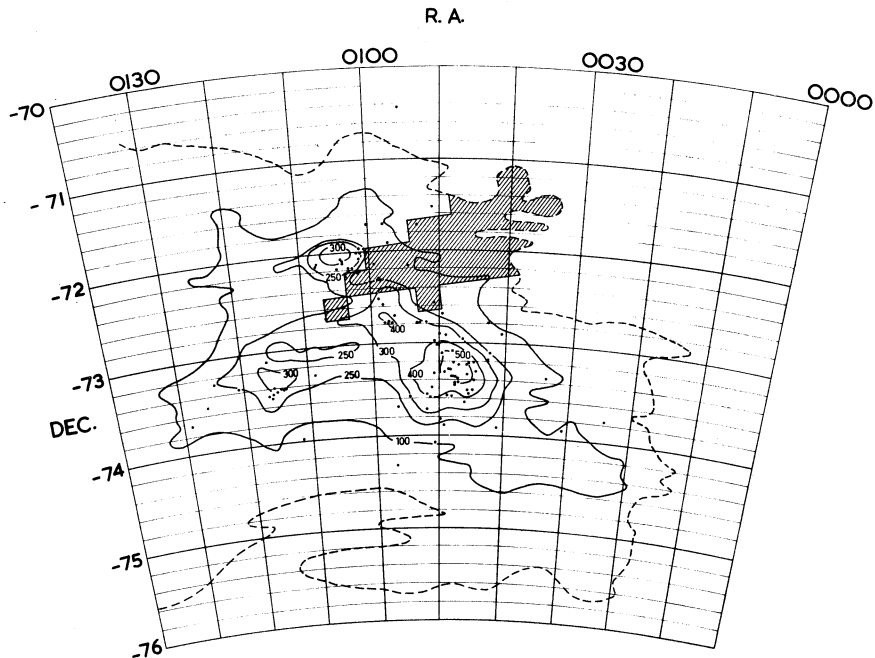


Fig. 4.—Contours of 21 cm H-line integrated brightness with the positions of HII regions from the Henize (1956) catalogue indicated (dots). The shaded area shows the region of high star-to-gas ratio.

There is a superficial correlation between the HII regions in the SMC, which are generally weak and small, and the gas concentrations shown in Figure 4. About half the total number of HII regions in the Henize (1956) catalogue are located in or near the neutral gas concentrations.

Velocity comparisons made by Bok *et al.* (1964) show only a loose connection between the profile peak velocities and the HII region velocities, giving the impression of small pockets of ionization somewhere in extended regions of gas.

(ii) *Comparisons with the LMC*

In strong contrast to the three broad gas concentrations in the SMC, the LMC has 52 clearly defined concentrations containing roughly the same total amount of

gas (McGee and Milton 1966). The peak temperatures of the LMC concentrations reach a maximum of 100°K and are generally less than 60°K , and there is a clear distinction between the concentrations and the rather tenuous background.

The maximum diameter of the LMC concentrations is 575 pc, and they range down to a lower limit of 200 pc set by the telescope resolution. There is a detailed correlation between the positions and velocities of the HII regions, the bright O and B stars, and the gas concentrations (McGee 1964), and very few HII regions lie outside HI concentrations.

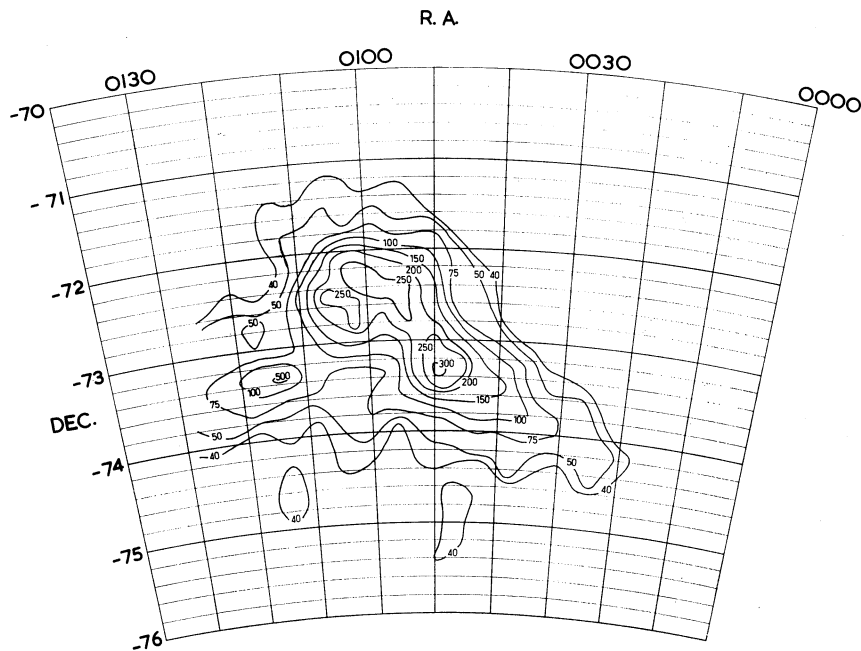


Fig. 5.—Contours of star counts to $m = 16$ from de Vaucouleurs (1955). Epoch of coordinates 1975. The contours have been redrawn to the linear star count scale; the numbers represent the star count in an area $17' \cdot 5$ arc square.

(iii) *The Bright Stars*

Figure 5 shows contours of star counts to $m = 16$ over areas $17' \cdot 5$ arc square by de Vaucouleurs (1955). Comparison with Figure 2 shows good correlation between the star distribution and that of the gas. The main body of the Cloud with its intense concentration at the south-west end is well marked in both sets of contours, as is the concentration in the wing near R.A. $01^{\text{h}} 15^{\text{m}}$, Dec. $-73^{\circ} 20'$.

A striking detail of the correlation is the extension in the south-west region centred on R.A. $00^{\text{h}} 30^{\text{m}}$, Dec. -74° , a region that is generally absent or inconspicuous in photographs of the SMC.

Figure 6 plots the correlation of the star counts with the average integrated brightness of the hydrogen radiation for areas $15'$ arc square. There is a fairly constant ratio between the star counts and the hydrogen integrated brightness over most of

the SMC, except for the points marked with crosses, which are confined to a small region of the Cloud centred on R.A. $00^{\text{h}} 50^{\text{m}}$, Dec. $-72^{\circ} 30'$. This area is shaded in Figure 4. In this small region there appear to be approximately twice as many bright stars relative to the amount of hydrogen; it contains the largest HII region in the SMC (N 66 in the Henize catalogue).

(iv) *Continuum Radiation*

Maps of continuum radiation at 20 cm (Mathewson and Healey 1964) and at 11 cm (Broten, personal communication) show a ridge of radiation extending from the main body of the Cloud through the area around R.A. $00^{\text{h}} 50^{\text{m}}$, Dec. $-72^{\circ} 30'$, referred to in subsection (iii) above.

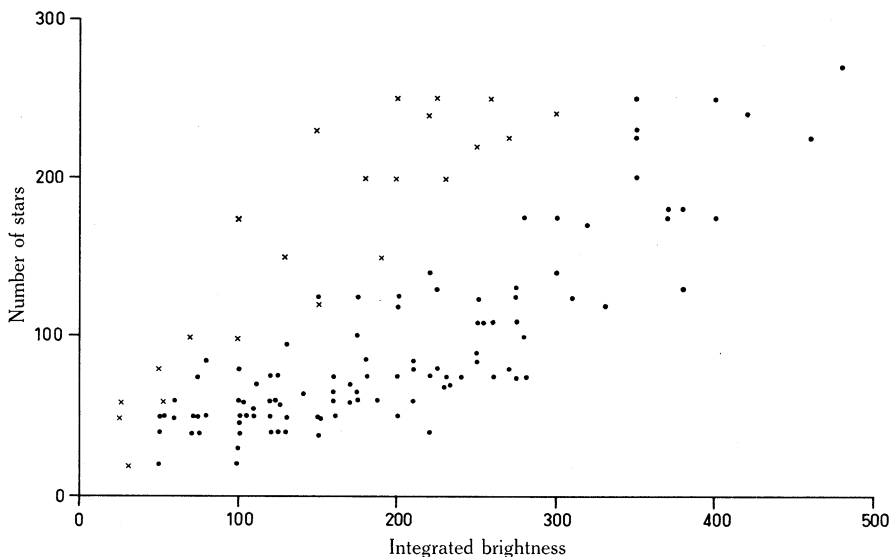


Fig. 6.—Correlation between star count and integrated hydrogen brightness. The crosses are points for a limited area centred on R.A. $00^{\text{h}} 50^{\text{m}}$, Dec. $-72^{\circ} 30'$.

(v) *Cepheids*

In Figure 7 the positions of over 1000 Cepheid* variable stars are plotted on the HI contours. It is obvious that though the gas and variables occupy the same general region there is no detailed correspondence between the gas concentrations and the stars. The result is similar if the details of Cepheid periods are included in the comparison.

This conclusion and that of subsection (iii) above are opposite to those of Ishida (1961) and Badalyan (1962), who have concluded, from the earlier survey of Kerr, Hindman, and Robinson (1954) that the Cepheid distribution is similar to that of the neutral hydrogen and that there is no connection between the bright stars and neutral hydrogen.

* The list of variables was compiled by Professor S. C. B. Gascoigne of the Australian National University, Canberra, who kindly made his tabulations available.

(vi) *Clusters*

Comparisons with cluster distributions of Lindsay (1958) and Kron (1956) do not yield any detailed correlation, although the position angle of the major axis of Lindsay's enclosing ellipse, 60° , is very close to the direction derived in Section VI(b) of the present paper for the plane of rotation of the galaxy.

V. INTERPRETATION OF THE VELOCITY DIAGRAMS

The velocity-R.A. diagrams were described in Section III(a). These diagrams may be interpreted as sections through the SMC with the velocity coordinate equivalent to distance, if, as in the case of our Galaxy, a relationship between distance and velocity can be established. The clear multi-peaked profiles in the SMC

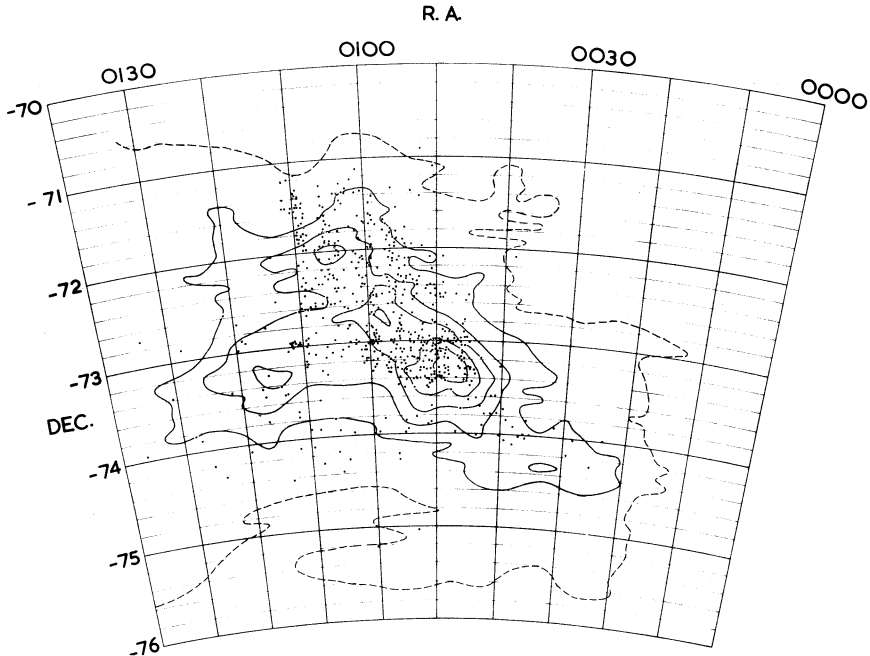


Fig. 7.—Contours of 21 cm H-line integrated brightness compared with the distribution of 1500 Cepheids.

observations would indicate the presence of relatively independent gas masses in the line of sight. An early interpretation of these multiple peaks on the basis of a limited number of profiles was that the peaks belonged to large masses of gas with independent spatial motions (Hindman 1964*a*). However, the increased amount of data now available in the velocity-R.A. diagrams show that the double-peaked features are concentrations within a larger continuous velocity range.

(a) *Gas Shells*

The form of the contours in the velocity-R.A. plane of Figure 8 and many similar diagrams suggests that they are due to an expanding shell-like structure.

The cross section of such a shell in a velocity–angular-distance plane will be an ellipse. Figure 9 shows the cross section in the velocity–declination plane at right angles to Figure 8 and through the apparent centre of the shell at R.A. 01^h 05^m.

It would be unlikely that such a large shell (almost 2 kpc in diameter) resulting from, say, an initial explosion, would preserve uniformity of shape and velocity, and the various sections (Figs. 8 and 9) would be modified by general motions of the galaxy, such as rotation. It is not surprising, therefore, that our shell shows some irregularities. Anticipating the results of Section VI on rotation, the direction of the maximum velocity gradient due to rotation is known, and Figure 10 shows the

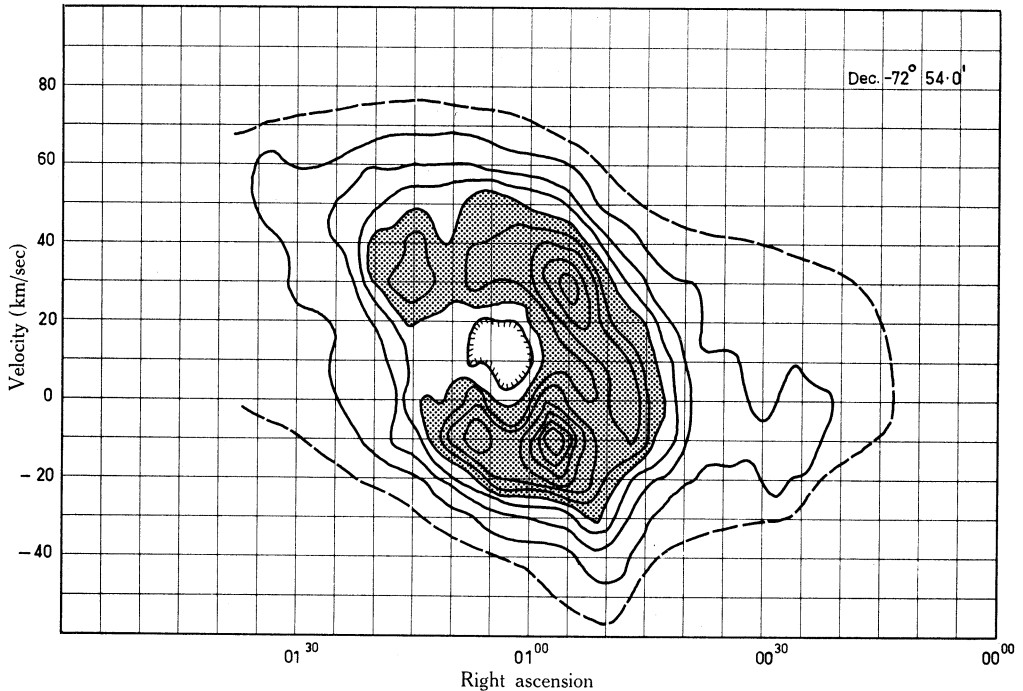


Fig. 8.—R.A.–velocity diagram for the constant declination track at Dec. $-72^{\circ} 54' \cdot 0$ (epoch 1963). The full contours have the values 5, 10, 15, etc. units, where 1 unit equals $1 \cdot 4$ degK aerial temperature; the outer (dashed) contour is an estimate of the limits of detectable radiation with the present receiver sensitivity. The shaded portion shows the ring-like distribution of the central contours.

velocity–angular-distance diagram at right angles to this direction. As might be expected, the diagram shows the maximum degree of symmetry. Details of the gas distribution along various diameters of the shell have been published by Hindman and Sinclair (1965).

That the shell is in expansion is known from previous work (Hindman 1964*b*) on the relation of the double-peak velocities to the velocity of the stars and interstellar absorption lines in these directions.

The shell just discussed is the most prominent of three such structures in the SMC, and the dashed circles in Figure 11 show the locations of these shells. Shell

No. 1, as we have seen, appears to be an almost complete sphere. Shell No. 2 is seen in the constant declination diagram of Figure 12. This shell has broken through to regions of low gas density on the northern and southern boundaries, and Figure 13 shows the most complete section through this shell. This section is tilted from the normal to the plane of the sky. A possible third shell, No. 3, is less well defined and appears to overlap Shell No. 1 near R.A. $01^{\text{h}} 15^{\text{m}}$ in the declination range -73° to $-73^{\circ} 30'$, in the wing of the Cloud. Figure 14 is a constant declination section through Shell No. 3.

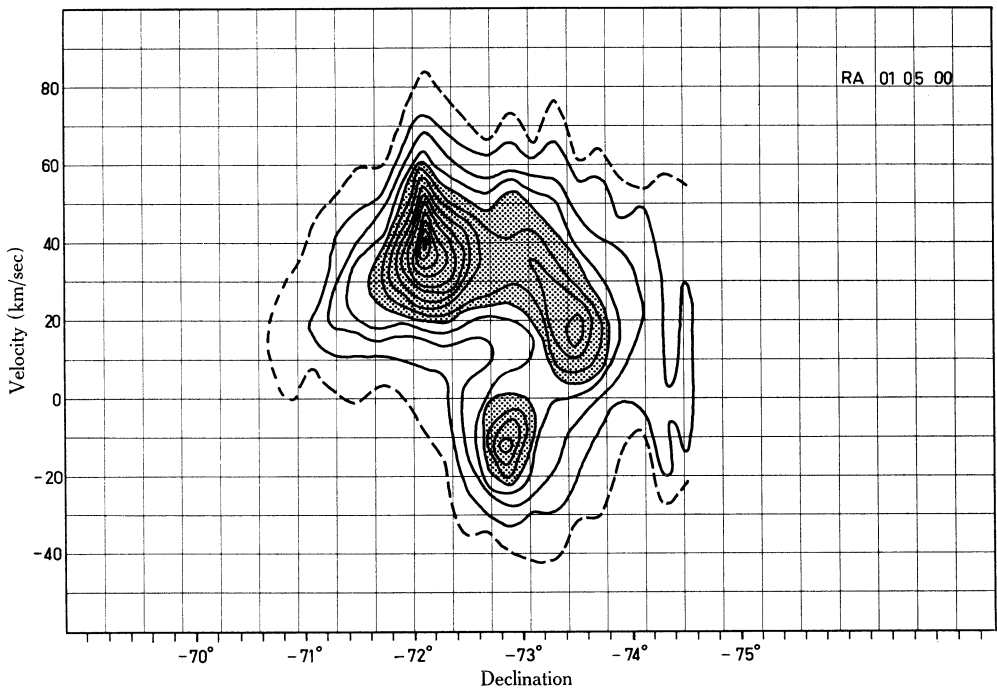


Fig. 9.—Declination-velocity contours for a constant right ascension track at R.A. 0105 showing ring-like structure (shaded).

Table 1 contains estimated parameters for the three shells mentioned. The mass of $1.9 \times 10^7 M_{\odot}$ estimated for the neutral gas of Shell No. 1 is of the same order as that for the proposed super supernova remnant of Westerlund and Mathewson (1966) in the LMC. Unlike the normal galactic supernova shell, these very large structures have no appreciable non-thermal radio emission. This, however, is not surprising, since the maximum age for the structures, assuming that the velocity of expansion has never been less than the present 25–30 km/sec, is of the order of 10^7 yr. This is several orders of magnitude greater than the oldest supernova remnants from which non-thermal radiation has been detected.

Large ring-like structures of 1–2 kpc diameter have been pointed out in a number of photographs of external galaxies by Hayward (1964), and it is possible that large structures of this type are a common feature of certain types of galaxies.

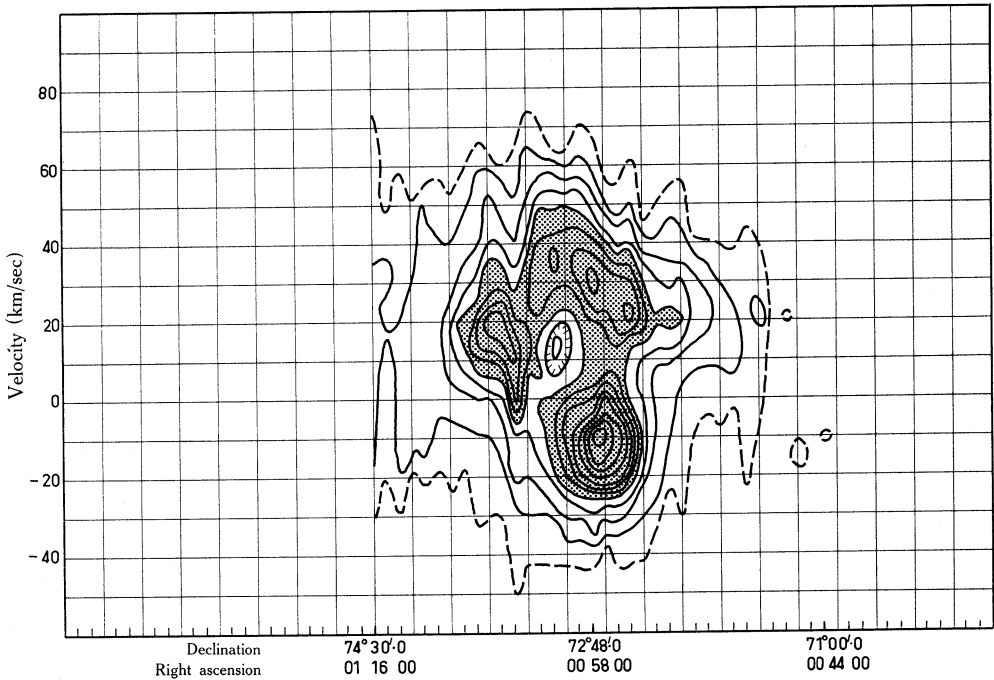


Fig. 10.—Contours for a section through the Cloud at right angles to the direction of maximum velocity gradient. The ring-like structure is shaded.

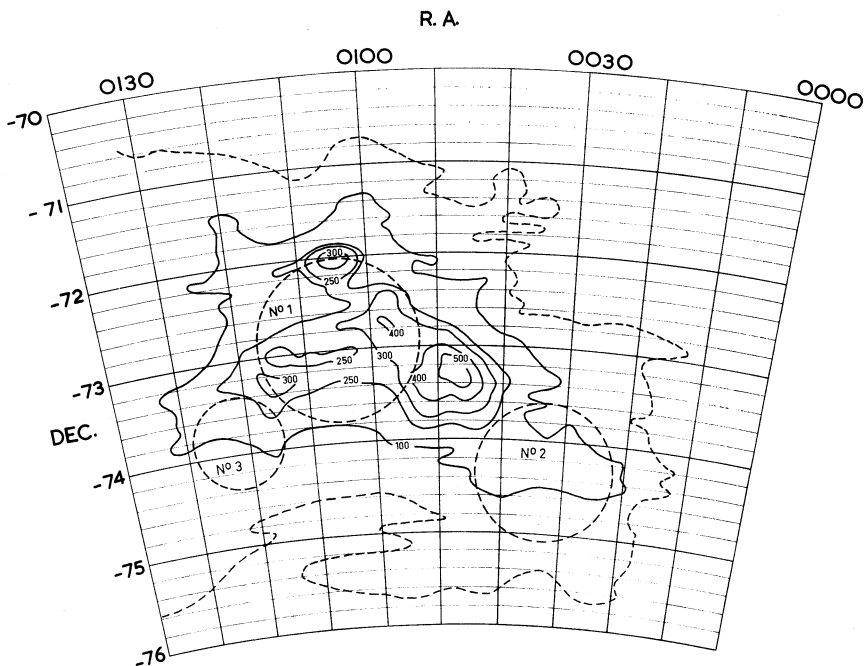


Fig. 11.—Contours of integrated brightness with the positions of three expanding shells of gas indicated (dashed circles).

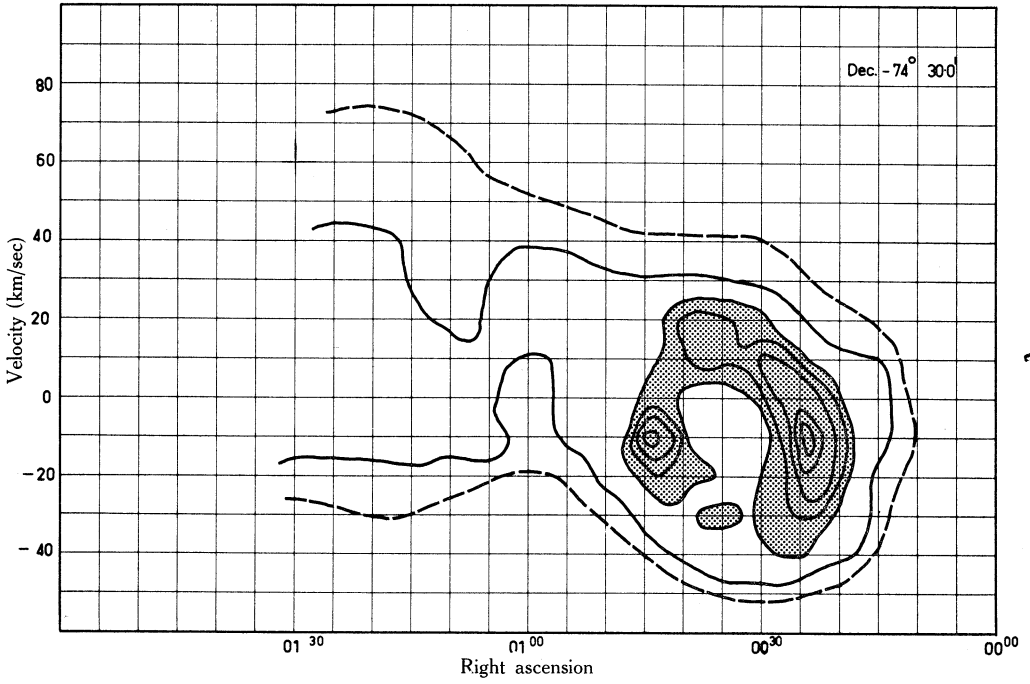


Fig. 12.—Constant declination section through Shell No. 2 at Dec. $-74^{\circ} 30' \cdot 0$, with the ring-like structure shaded.

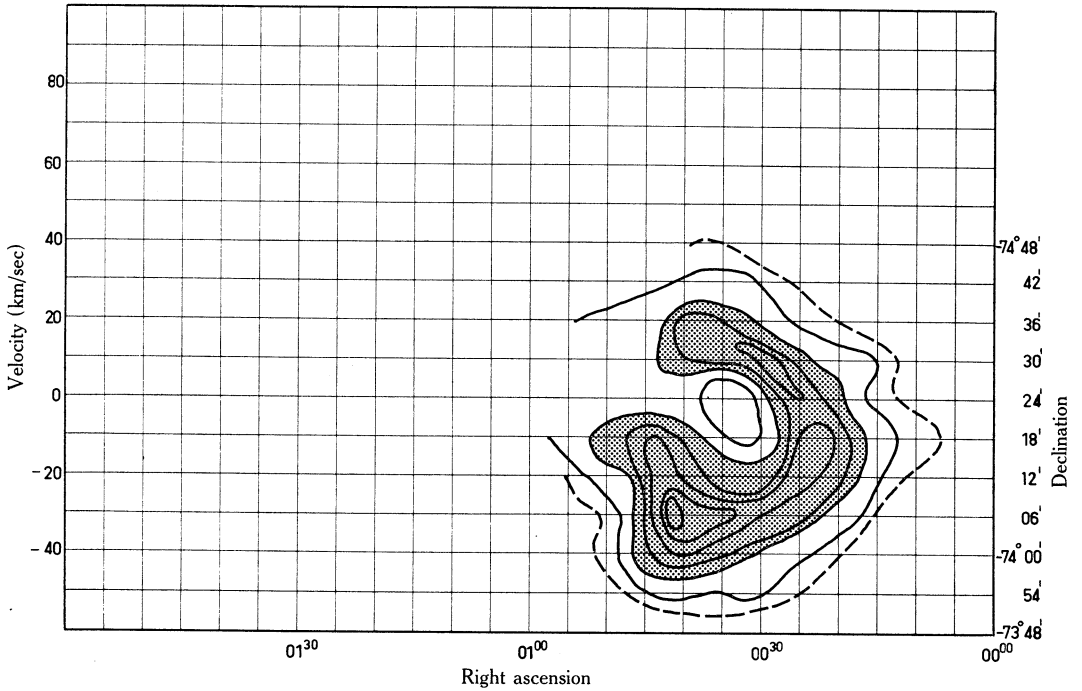


Fig. 13.—A tilted section through Shell No. 2 showing the almost complete ring in a plane tilted to the line of sight. The ring is shaded.

The only evidence of the shells in the stellar distribution is an arc of stars and HII regions, delineated by Rodgers (1959), that combine to form the north-east section of the Cloud body and the wing concentration near R.A. $01^{\text{h}} 15^{\text{m}}$, Dec. $-73^{\circ} 20'$, all of which lie on the periphery of the main shell.

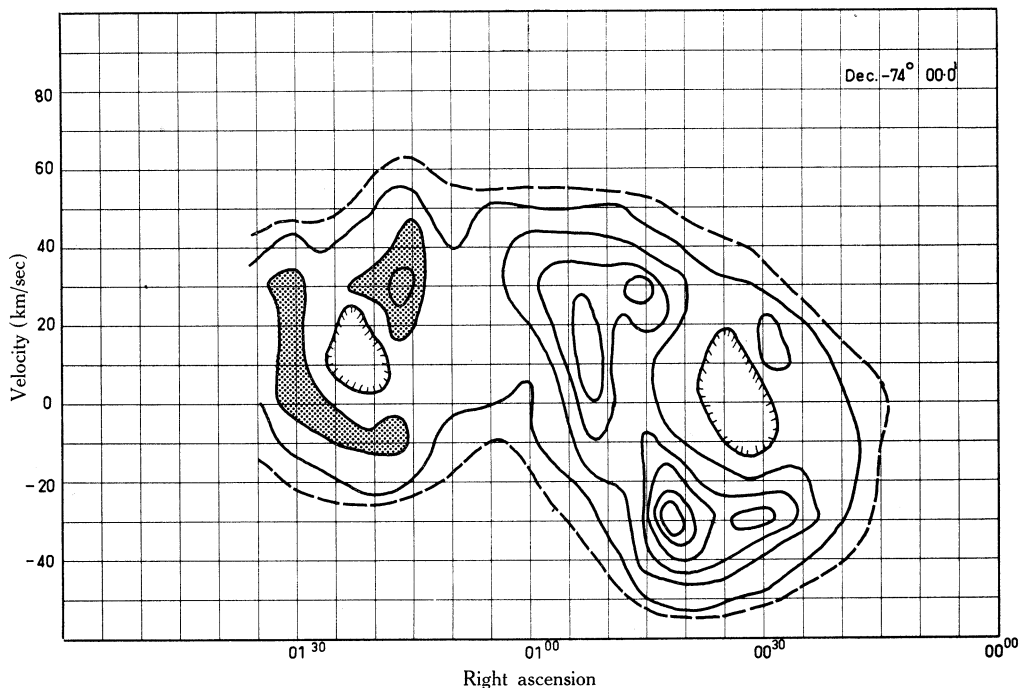


Fig. 14.—Constant declination section through Shell No. 3 at Dec. $-74^{\circ} 00' \cdot 0$.

TABLE 1
DETAILS OF THREE EXPANDING SHELLS IN THE SMC

Shell No.	R.A.	Dec. (centre)	Velocity (km/sec)	Diameter	Expansion Velocity (km/sec)	Hydrogen Mass (M_{\odot})	Max. Density (atoms/cm ³)	Percentage of Total HI
1	0105	$-72^{\circ} 54'$	+15	$1^{\circ} \cdot 8$	23	$1 \cdot 9 \times 10^7$	1.2	4%
2	0033	$-74^{\circ} 20'$	-15	$1^{\circ} \cdot 5$	21	$1 \cdot 0 \times 10^7$	0.6	2%
3	0122	$-73^{\circ} 54'$	+10	$1^{\circ} \cdot 0$	19	$0 \cdot 3 \times 10^7$	0.4	1%

(b) *The SMC Bar*

The main peak of the integrated brightness diagram occurs at R.A. $00^{\text{h}} 48^{\text{m}}$, Dec. $-73^{\circ} 18'$ (Section IV). In this position the peak brightness temperature of the profile reaches 150°K , and in Figure 15 the velocity-R.A. diagram, which includes the point of maximum integrated brightness, shows a very wide velocity distribution

at this point. The very high temperature considerably exceeds that at any other point in either the LMC or the SMC and is only just surpassed at two or three points in the Galaxy (Kerr and Hindman, unpublished data).

The high temperature and the velocity dispersion suggest that this small region is of a very special nature. A further anomaly is the recent discovery by Basinski, Bok, and Bok (1967) of large numbers of very blue stars in this region. The integrated colour of this region has been found by Hogg (1955) to be very blue relative to the rest of the SMC. The high temperature and wide velocity spread are consistent with

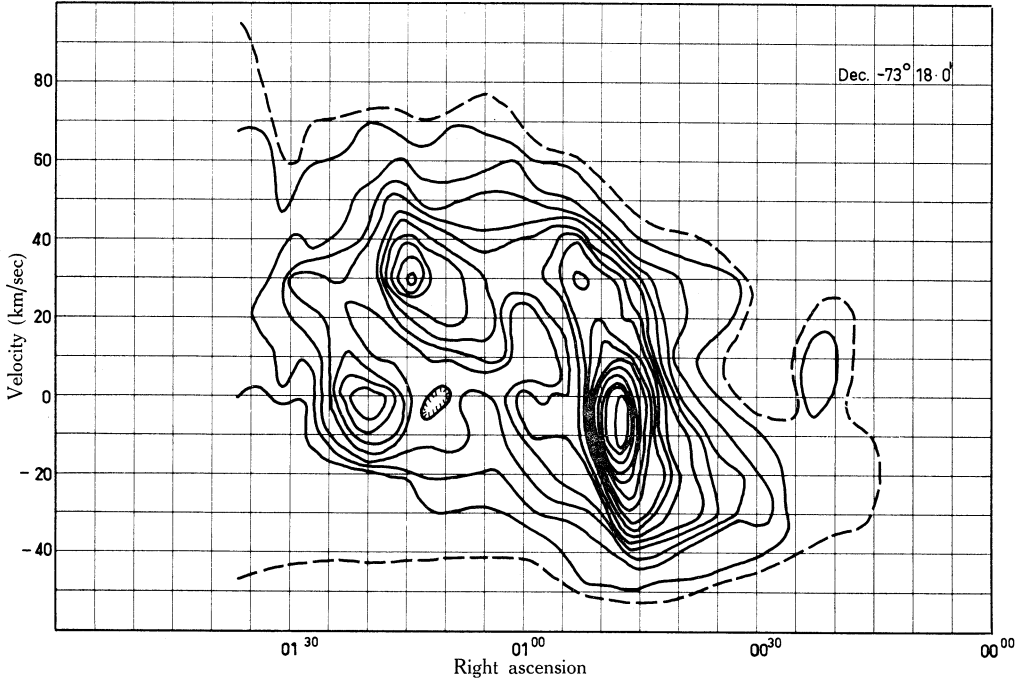


Fig. 15.—R.A.-velocity contour diagram at Dec. $-73^{\circ} 18' 0$. This constant declination diagram passes through the integrated brightness maximum at R.A. 0048, Dec. $-73^{\circ} 18' 0$, and shows the wide spread of velocity associated with this maximum.

a considerable depth of gas, and it is suggested that if the Small Cloud contains a bar it may lie almost in the line of sight at this point. However, the properties of this bar would be in direct contrast with the known properties of the LMC bar, where the stellar population tends to be old and there is no marked gas concentration.

Perhaps, alternatively, this feature might be looked upon as a very turbulent nucleus in the SMC gas.

VI. ROTATION CURVE

(a) *Velocity Corrections*

As noted in Section III(d) all velocity observations for this paper have been corrected for the Earth's orbital motion, the standard solar motion relative to the local standard of rest, and a galactic rotation component. The dashed lines on Figure

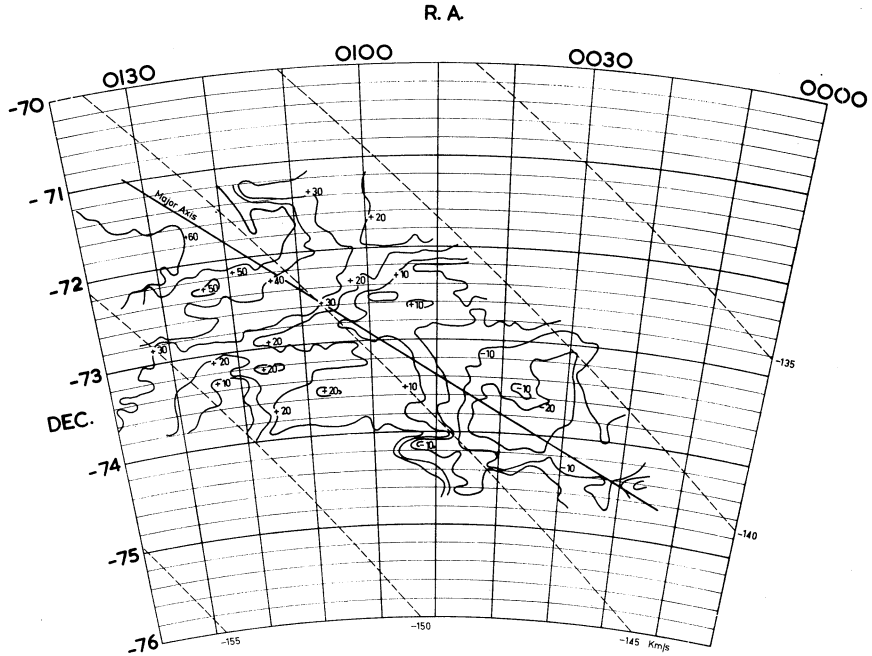


Fig. 16.—Contours of constant median velocity over the area of the SMC, with applied velocity corrections for motion of the Sun and rotation of the Galaxy indicated by the dashed lines. The major axis of the SMC rotation ellipse is also shown (heavy line).

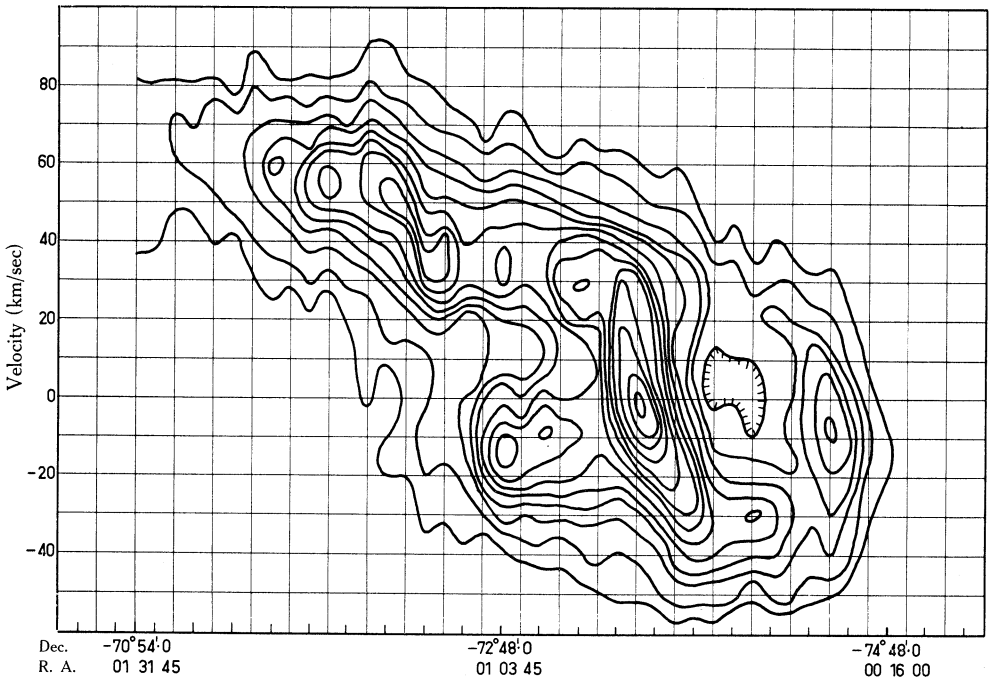


Fig. 17.—Velocity-angular-distance contours along a track almost coincident with the SMC major axis.

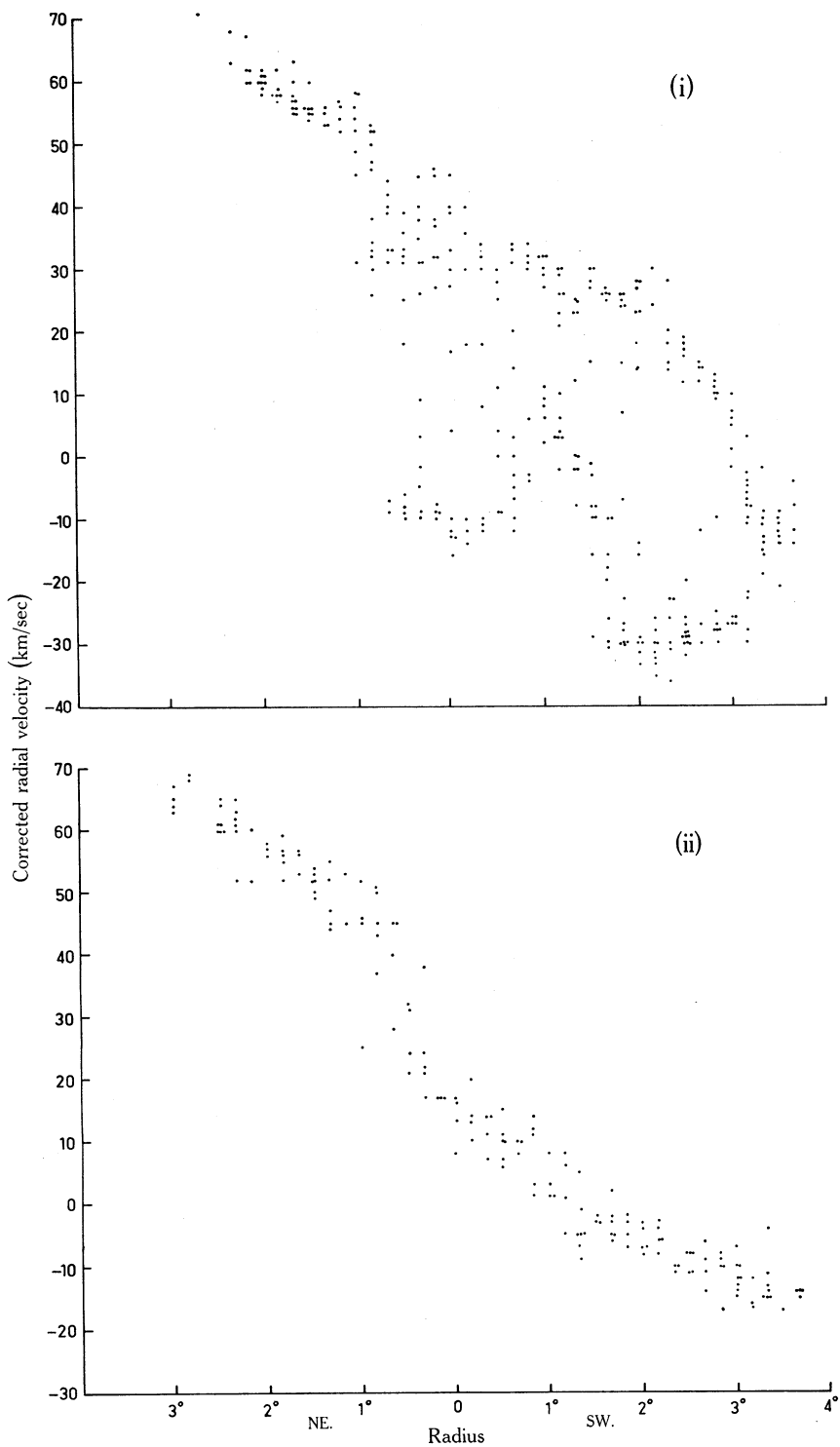


Fig. 18

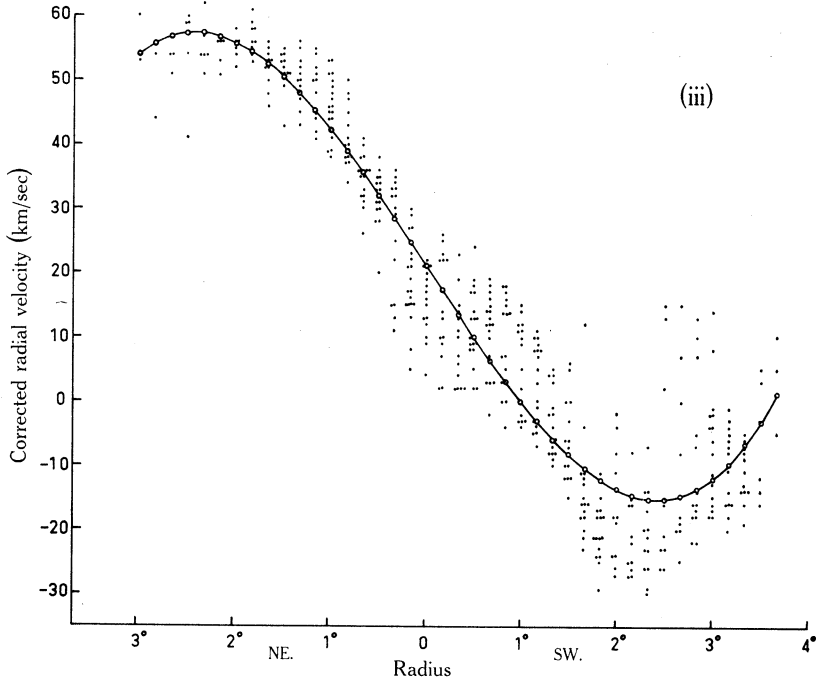


Fig. 18 (continued)

16 are contours showing the correction applied for the combined effect of solar motion and galactic rotation. Changing the value of the galactic rotation component from 216 km/sec to the more recently adopted 250 km/sec increases the corrections by approximately 20 km/sec, and this change varies less than 2 km/sec across the area of the SMC. We may, therefore, assume that the velocity pattern for the SMC will remain unchanged for any reasonable value of galactic rotation correction.

(b) *The Rotation Ellipse*

For a flattened rotating system the velocity pattern usually shows a strong gradient along the major axis. Examination of the velocity distribution in the form of contours of median velocity (Fig. 16) shows a clear gradient from north-east to south-west across the Cloud. It was assumed that this gradient indicated rotation of the SMC, though it could in part be due to other motions, including a binary motion of the SMC and LMC and possibly translational motion at an angle to the line of sight. The major axis indicated in Figure 16 was chosen taking into account the greatest elongation of the gas contours, the symmetry of the gas contours, and the distinct

Fig. 18.—Plots of the velocity distribution along the major axis of the SMC. (i) velocities from the profile peaks; (ii) mean profile velocities; (iii) median profile velocities and the rotation curve derived from the median velocities. The centre of symmetry of the rotation curve is at R.A. 0103, Dec. $-72^{\circ} 45' 0$. The points are from a band $\frac{1}{2}^{\circ}$ on either side of the major axis, which lies in position angle 55° through the centre of the rotation curve. In groups (i) and (ii) not all the observed points have been included, but in group (iii) all observed points have been plotted.

minimum in the velocity distribution near R.A. $00^{\text{h}} 35^{\text{m}}$ and Dec. -74° . It lies in position angle 55° through the point $01^{\text{h}} 03^{\text{m}}$ R.A. and $-72^{\circ} 45' \cdot 0$ Dec., the centre of the final rotation curve.

(c) *Tilt of the SMC*

For any appreciable tilt of a flattened rotating system the velocity pattern shown in Figure 16 would be expected to show a decreasing velocity with distance from the major axis. However, the contours show little evidence of such a decrease.

The other generally used method of determining the tilt of a galaxy from the axial ratio of the ellipse formed by the outer isophotes when applied to the present data gives an axial ratio of greater than 3 : 1, leading to a maximum tilt from the line of sight of less than 20° . The diameter of the central expanding shell is 1.8 kpc, and this is more than half the estimated minor-axis dimension. It is to be expected that the thickness of the galaxy will not be less than the diameter of the shell, so that the tilt may be much less than 20° .

(d) *Rotation Curve*

The problem of deriving a rotation curve for the SMC is complicated by the peculiar internal motions due to the expanding shells and the turbulence in the region of the suggested bar or nucleus. Figure 17 is a velocity-angular-distance diagram for a track lying almost along the major axis of the system, and it clearly demonstrates the presence of large-scale motions other than rotation.

Plots of the velocity data in a band $\pm \frac{1}{2}^{\circ}$ from the major axis are shown in Figure 18. Figure 18(i) is a plot of the velocities of the profile peaks, (ii) shows the mean velocities of the profiles and (iii) the median velocity values. The peak points do not define any reasonable curve, but the mean and median points are more promising.

A curve-fitting programme used to fit a third-order polynomial to these sets of points gives a reasonable curve for the median points, as shown in Figure 18(iii). However, the curve fitted in this way to the mean points does not exhibit a second turnover in the range of the diagram, and this is due mainly to the effect of the discontinuity 1° on the north-east side where the edge of the main expanding shell occurs.

The curve fitted to the median points is symmetrical about R.A. $01^{\text{h}} 03^{\text{m}}$ and Dec. $-72^{\circ} 45'$ with a systemic velocity of $+21$ km/sec. This is very close to the centre of expanding Shell No. 1 at R.A. $01^{\text{h}} 05^{\text{m}}$ and Dec. -73° with a velocity of $+15$ km/sec.

The rotation curve need not necessarily be symmetrical. Many instances of asymmetrical curves exist, e.g. the LMC (McGee and Milton 1966) and our own Galaxy (Kerr 1964). The points from which the curve is derived certainly would lend themselves to an asymmetrical interpretation.

The centre of rotation of the symmetrical curve is displaced about 1 kpc from the centre of mass of the SMC. A similar relationship has been found for NGC 55 (Robinson and van Damme 1966) and the LMC.

(e) *Total Mass*

We have not been able to define the rotation curve much beyond the turnover points, so that fitting of a rotation curve for any of the standard models, such as those discussed by Wyse and Mayall (1942), Perek (1948, 1950), and others, is not possible.

We can, however, calculate the mass for a thin disk inside the radius of maximum rotational velocity, thus,

$$M_R = \frac{V^2 R}{G},$$

and make some allowance for the thickness of the disk and the fact that our idealized curve probably underestimates the peak rotation velocity.

From the rotation curve we have

$$V = 36 \text{ km/sec}, \quad R = 2^\circ \cdot 5 = 2 \cdot 6 \text{ kpc},$$

which gives

$$M_R = 0 \cdot 7 \times 10^9 M_\odot.$$

Various estimates of the effect of layer thickness have been made by Kerr and de Vaucouleurs (1956) and Brandt (1960), and for a galaxy with an axial ratio of thickness to diameter of approximately 1 : 3 an allowance of 20% extra mass seems reasonable.

It is possible only to guess at the reduction in the rotation curve peak velocity, but we can see in Figure 18 that at the north-east end of the major axis, where there are no obvious internal cloud motions, the peak velocities are about 10 km/sec higher than the median values. Correcting for these two effects leads to a rotationally supported mass of $1 \cdot 3 \times 10^9 M_\odot$.

Random motions further complicate the mass calculation, but in the case of the SMC this is probably a small correction.

The virial theorem (Chandrasekhar 1942) gives

$$M = \frac{2 \bar{V}^2 R}{G}$$

for a spherical system with only random motions, where

$$\bar{V}^2 = \bar{u}^2 + \bar{v}^2 + \bar{w}^2 = 3\bar{w}^2$$

and R is the effective radius of the random motions, which will be assumed to be a measure of the Z thickness of the gas layer. For the SMC, $R = 1$ kpc.

The observed half-widths of single peak components of the profiles vary between 12 and 40 km/sec, with the most frequent width 25 ± 5 km/sec, equal to a mean dispersion of $\pm 10 \cdot 5$ km/sec, slightly less than the figure of 11·5 km/sec quoted by McGee and Milton (1966) for the LMC.

From the measured dispersion in the profile peaks $(\bar{w}^2)^{\frac{1}{2}} = 10 \cdot 5$ km/sec, so that $3\bar{w}^2 = 330$ and the mass supported by random motions is then $0 \cdot 15 \times 10^9 M_\odot$.

With all corrections, the final estimated total mass for the SMC inside a radius of 2.6 kpc is

$$M_T = (1.5 \pm 0.3) \times 10^9 M_\odot,$$

which is not greatly different from the value of $1.3 \times 10^9 M_\odot$ estimated by Kerr and de Vaucouleurs (1956) with an assumed distance to the SMC of 46 kpc.

Various quantities derived from the mass of the SMC are listed in Table 2, with corresponding values for the LMC derived from the results of McGee and Milton (1966). The extremely high value 0.32 of M_H/M_T as compared with 0.09 for the LMC probably indicates a very much slower rate of development for the SMC rather than a younger system, since the gas link between the LMC and SMC would seem to indicate a common origin for the two systems.

TABLE 2
COMPARISON OF MASSES AND LUMINOSITIES OF THE LMC AND SMC

	M_T (M_\odot)	M_H (M_\odot)	M_H/M_T	M_H/L	M_T/L
LMC	6.1×10^9	5.4×10^8	0.09	0.17	1.9
SMC	1.5×10^9	4.8×10^8	0.32	0.85	2.5

VII. CONCLUSIONS

This high resolution survey of the SMC confirms earlier measurements of neutral gas content and strikingly contrasts the smooth gas distribution of the SMC with that of the LMC, which is extremely patchy.

The SMC is a slightly flattened system, rotating in a plane edge-on to the observer. Three broad structural features have been distinguished which may represent expanding shells of gas within the main body of the cloud. These shells contain masses of gas comparable with super supernova shells detected in the LMC.

The rotation curve derived from the detailed velocity distribution has been used to estimate a mass for the Cloud of $1.5 \times 10^9 M_\odot$.

VIII. ACKNOWLEDGMENTS

I would like to thank Professor B. J. Bok, Professor S. C. B. Gascoigne, and Dr. B. E. Westerlund of Mount Stromlo Observatory for helpful discussions. Dr. F. J. Kerr and Mr. R. X. McGee have provided many useful comments, and Mr. J. G. Bolton has helped greatly by reading and criticizing the manuscript.

IX. REFERENCES

- BADALYAN, G. (1962).—*Dokl. Akad. Nauk armyan. SSR* **35**, 21.
 BASINSKI, J. M., BOK, B. J., and BOK, P. F. (1967).—A colour magnitude array for a region in the core of the Small Magellanic Cloud. *Mon. Not. R. astr. Soc.* (in press).
 BOK, B. J., GOLLNOW, H., HINDMAN, J. V., and MOWAT, M. (1964).—*Aust. J. Phys.* **17**, 404.
 BRANDT, J. C. (1960).—*Astrophys. J.* **131**, 293.
 CHANDRASEKHAR, S. (1942).—“Principles of Stellar Dynamics.” p. 200. (Univ. of Chicago Press.)

- GASCOIGNE, S. C. B., and KRON, G. E. (1965).—*Mon. Not. R. astr. Soc.* **130**, 333.
- HAYWARD, R. (1964).—*Publs astr. Soc. Pacif.* **76**, 35.
- HENIZE, K. G. (1956).—*Astrophys. J. Suppl. Ser.* **2**, 315.
- HINDMAN, J. V. (1964a).—Symp. IAU-URSI No. 20 (Canberra 1963). p. 255.
- HINDMAN, J. V. (1964b).—*Nature, Lond.* **202**, 377.
- HINDMAN, J. V., and BALNAVES, K. M. (1967).—*Aust. J. Phys. Astrophys. Suppl.* No. 4.
- HINDMAN, J. V., KERR, F. J., and MCGEE, R. X. (1963).—*Aust. J. Phys.* **16**, 570.
- HINDMAN, J. V., MCGEE, R. X., CARTER, A. W. L., HOLMES, E. C. J., and BEARD, M. (1963).—*Aust. J. Phys.* **16**, 552.
- HINDMAN, J. V., and SINCLAIR, M. W. (1965).—Mount Stromlo Symposium on the Magellanic Clouds, 1965. p. 76. (Mount Stromlo Observatory: Canberra.)
- HOGG, A. R. (1955).—*Mon. Not. R. astr. Soc.* **115**, 473.
- ISHIDA, K. (1961).—*Publs astr. Soc. Japan* **13**, 87.
- JOHNSON, H. M. (1961).—*Publs astr. Soc. Pacif.* **73**, 20.
- KERR, F. J. (1964).—Symp. IAU-URSI No. 20 (Canberra 1963). p. 81.
- KERR, F. J., HINDMAN, J. V., and ROBINSON, B. J. (1954).—*Aust. J. Phys.* **7**, 297.
- KERR, F. J., and DE VAUCOULEURS, G. (1956).—*Aust. J. Phys.* **9**, 90.
- KRON, G. E. (1956).—*Publs astr. Soc. Pacif.* **68**, 125.
- LINDSAY, E. M. (1958).—*Mon. Not. R. astr. Soc.* **118**, 172.
- MCGEE, R. X. (1964).—*Aust. J. Phys.* **17**, 515.
- MCGEE, R. X., and MILTON, JANICE A. (1966).—*Aust. J. Phys.* **19**, 343.
- MCGEE, R. X., and MURRAY, J. D. (1963).—*Proc. Instn Radio Engrs Aust.* **24**, 191.
- MATHEWSON, D. S., and HEALEY, J. R. (1964).—Symp. IAU-URSI No. 20 (Canberra 1963). p. 245.
- PEREK, L. (1948).—*Contr. astr. Inst. Masaryk Univ.* **1**(6), 1.
- PEREK, L. (1950).—*Bull. astr. Insts Csl.* **2**, 75.
- ROBINSON, B. J., and VAN DAMME, K. J. (1966).—*Aust. J. Phys.* **19**, 111.
- RODGERS, A. W. (1959).—*Observatory* **79**, 49.
- DE VAUCOULEURS, G. (1955).—*Astr. J.* **60**, 219.
- WESTERLUND, B. E., and MATHEWSON, D. E. (1966).—*Mon. Not. R. astr. Soc.* **131**, 371.
- WYSE, A. B., and MAYALL, N. U. (1942).—*Astrophys. J.* **95**, 24.

